



Data-driven discovery of a universal indicator for metallic glass forming ability

Ming-Xing Li^{1,2,6}, Yi-Tao Sun^{1,6}, Chao Wang^{1,6}, Li-Wei Hu¹, Sungwoo Sohn³, Jan Schroers^{1,2,4,5} and Yan-Hui Liu^{1,2,4,5} ✉

Despite the importance of glass forming ability as a major alloy characteristic, it is poorly understood and its quantification has been experimentally laborious and computationally challenging. Here, we uncover that the glass forming ability of an alloy is represented in its amorphous structure far away from equilibrium, which can be exposed by conventional X-ray diffraction. Specifically, we fabricated roughly 5,700 alloys from 12 alloy systems and characterized the full-width at half-maximum, Δq , of the first diffraction peak in the X-ray diffraction pattern. A strong correlation between high glass forming ability and a large Δq was found. This correlation indicates that a large dispersion of structural units comprising the amorphous structure is the universal indicator for high metallic glass formation. When paired with combinatorial synthesis, the correlation enhances throughput by up to 100 times compared to today's state-of-the-art combinatorial methods and will facilitate the discovery of bulk metallic glasses.

It is generally believed that any metal or alloy can be formed into a glass^{1–4}, and the ease with which an alloy forms a glass is referred to as the glass forming ability (GFA). Because direct determination of GFA requires elaborate measurements^{5,6}, indirect criteria to estimate GFA have been proposed^{5,7}. However, such criteria are either non-quantitative⁸ or include quantities that require an elaborate measurement process^{4,7}. Although investigations via computations have suggested that glass formation of an alloy is affected by short-range ordering and their interconnectivity^{9–12}, a general correlation between structure and GFA remains elusive.

Besides their scientific importance for glass and liquid-state physics^{1,3}, bulk metallic glasses (BMGs) also possess exciting characteristics for technological use¹³. Their combination of mechanical properties with plastic-like processability suggests immense potential for many structural and functional applications^{14,15}. Nevertheless, this combination has thus far been realized in very few alloys. As a consequence, today's use of BMGs is limited to highly specialized applications. To unleash their potential, a much wider range of alloys must be characterized from the potential metallic glass forming composition space¹⁶.

Combinatorial methods have been developed and applied to determine some composition-dependent properties of metallic glasses, including high glass transition temperatures¹⁷, thermal plastic processability¹⁸, corrosion resistance¹⁹, phase transformations^{20–22} and hardness^{23,24}. As fast screening methods, X-ray diffraction (XRD) has been used broadly to identify the glass forming compositional range^{17,18,24,25}. However, such a range during sputtering in an alloy system that contains BMG-forming alloys is very large^{17,18,25}. This limits the effectiveness of the technique in reducing the number of alloys for the formation of BMGs. A breakthrough approach should be able to distinguish relative GFA among amorphous alloys in their as-sputtered state.

We have accomplished this in our work. We fabricated alloy libraries and characterized the composition-dependent structure

through XRD mapping, which results in roughly 5,700 XRD diffraction patterns from 12 alloy systems. By analysing such an unprecedented number of experimental data, both in quantity and in consistent quality, we found that a larger full-width at half-maximum (Δq) of the first diffraction peak in the XRD pattern correlated with a higher GFA within an alloy system. The Δq -GFA correlation suggests Δq as a universal and practical indicator for GFA. Supported by systematic molecular dynamics simulations, the Δq -GFA correlation also suggests that GFA is rooted in the dispersity of structural units comprising the amorphous structure.

Even though many BMGs are multicomponent alloys, they often behave in a pseudo-binary or -ternary manner due to the similarity of some of the alloy constituents⁶. To adequately represent BMG-forming alloy systems, we considered different binary and ternary alloy systems, for example, CuZr, NiTa, NiNb, ZrCuAl, ZrCuAg, ZrCuTi, ZrNiAl, IrNiTa, NiNbZr, GdCoAl, MgCuY and PdCuSi. The systems, comprising alkaline-earth metals, transition metals, rare earth elements and metalloids, have been widely studied and alloys of highest GFA in each of the here-considered systems are identified.

We synthesized the alloy libraries using magnetron cosputtering^{17,18} (Fig. 1a). The high effective cooling rate during sputtering deposition²⁶ results in vitrification in a wide composition range^{17,18,25}, so that the general tendency of glass formation can be revealed. Since all alloys within one library are fabricated under consistent conditions, they are suited for a relative comparison. The chemical composition for each alloy within the library is determined using energy dispersive X-ray spectroscopy (EDX), and XRD is used to determine the diffraction pattern for each alloy (Fig. 1b). Here we focus on the first diffraction peak within the XRD pattern. Analyses of all the collected XRD patterns revealed that 1,893 out of 5,727 alloys form glasses (see Supplementary Information for the classification of glassy and crystalline alloys). A key distinct feature is that Δq and also peak position varies among the amorphous

¹Institute of Physics, Chinese Academy of Sciences, Beijing, China. ²Songshan Lake Materials Laboratory, Dongguan, Guangdong, China. ³Department of Mechanical Engineering and Materials Science, Yale University, New Haven, CT, USA. ⁴Center of Materials Science and Optoelectronics Engineering, University of Chinese Academy of Sciences, Beijing, China. ⁵Beijing Advanced Innovation Center for Materials Genome Engineering, Beijing, China.

⁶These authors contributed equally: Ming-Xing Li, Yi-Tao Sun, Chao Wang. ✉e-mail: yanhui.liu@iphy.ac.cn

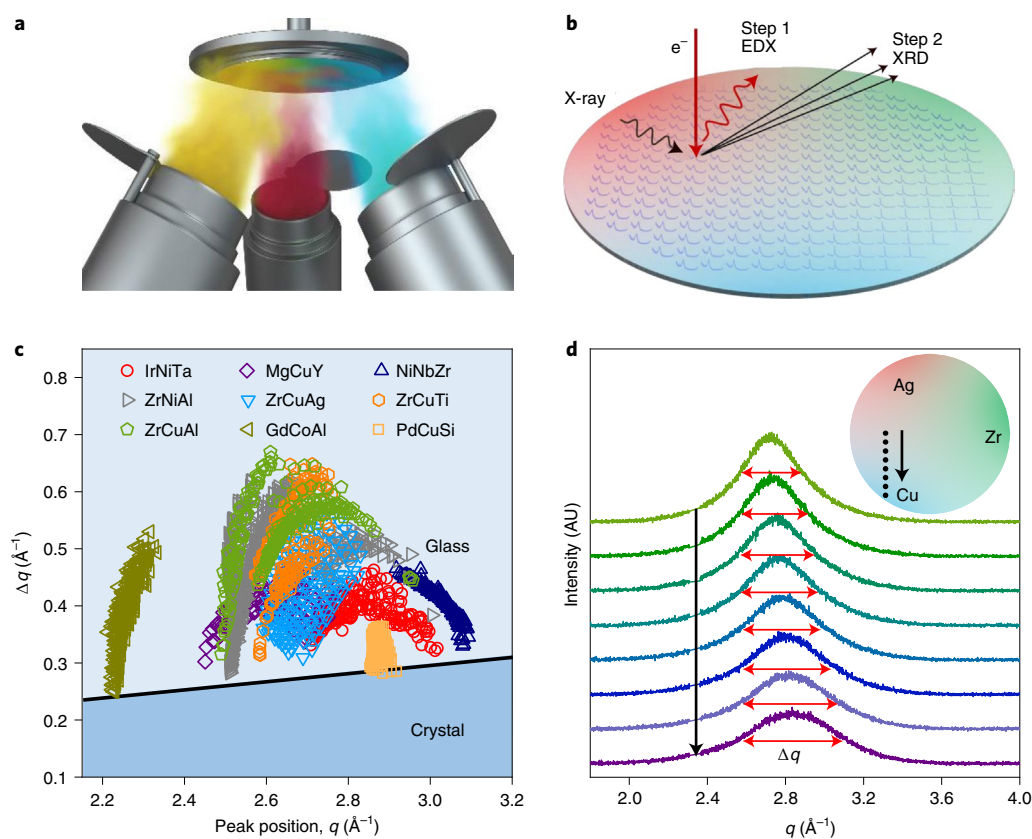


Fig. 1 | Flow chart illustrating the present combinatorial method and the obtained dataset. a–c, The entire procedure includes combinatorial synthesis by magnetron cosputtering (**a**), followed by automatic chemical analysis by EDX, XRD mapping and automatic data processing with a batch processing code (**b**), which results in a summary of peak position, q , and peak width Δq of the first diffraction peak for each of the alloy systems considered here (**c**). The diffraction angle 2θ was converted to momentum vector q via $q = 4\pi \times \sin\theta/\lambda$, where λ is the X-ray wavelength. According to the spread of Δq and q , the light blue area in **c** is considered to be glassy area. The solid line is drawn as a guide for the eyes. **d,** XRD patterns along the dots taken in ZrCuAg combinatorial library, showing the obvious change in Δq and peak position with the alloy composition.

alloys within the library. Within one alloy system, the amorphous alloys exhibit a broad variation of Δq with some variation in peak position (Fig. 1c). For example, for GdCoAl, Δq monotonically increases from 0.25 for $\text{Gd}_{83.3}\text{Co}_{6.3}\text{Al}_{10.4}$ to 0.53 for $\text{Gd}_{53.8}\text{Co}_{28}\text{Al}_{18.2}$. In other systems such as ZrCuAl, Δq first increases with increasing peak position from 0.32 for $\text{Zr}_{74.8}\text{Cu}_{16.6}\text{Al}_{8.6}$ to a maximum of 0.67 for $\text{Zr}_{48}\text{Cu}_{44}\text{Al}_8$, and subsequently decreases to 0.44 for $\text{Zr}_{26.7}\text{Cu}_{65.6}\text{Al}_{7.7}$. For each alloy system, there exists a smallest Δq , below which either crystalline Bragg peaks are present in the XRD patterns or the diffraction peaks are asymmetric, suggesting at least partial crystallization of the alloys (see Supplementary Information for details).

We now demonstrate that Δq and GFA are correlated within an alloy system. To do this, we compare the compositional dependence of Δq . Figure 1d presents the XRD patterns of glass forming alloys in a ZrCuAg combinatorial library, along the line marked in the inset. Although all of the alloys are amorphous, their first diffraction peaks differ and gradually increase in Δq from the Ag-rich towards the Cu-rich side. The composition of maximum Δq coincides with the compositions of best-known glass formers (Fig. 2). In fact, for the nine ternary alloy systems considered here (Fig. 2a–i) and three binary alloy systems (Fig. 2j–l), the composition of highest GFA within one alloy system^{17,27–31} always coincides with the composition where Δq is maximum within the system. We confirmed that the variation of Δq does not originate from residual stresses, difference in film thickness, or growth mode in the deposited films (Supplementary Information and Supplementary Figs. 7–9). The correlation of Δq and GFA within an alloy system

allows us to conclude that the GFA of an alloy is represented by its atomic structure reflected in Δq . Although this is not a general correlation from one alloy system to another, it has substantial ramifications for the development of metallic glasses and glass science.

For example, IrNiTa is an alloy system that has been explored for BMGs that can be used at high temperatures¹⁷. The previously reported BMG former in this system, $\text{Ir}_{33}\text{Ni}_{28}\text{Ta}_{39}$, can be cast into fully amorphous rods with diameters of up to 3 mm. Plotting Δq as a function of composition reveals that the alloys with the largest Δq exhibit different compositions of $\text{Ir}_{10}\text{Ni}_{55}\text{Ta}_{35}$ and $\text{Ir}_{10}\text{Ni}_{50}\text{Ta}_{40}$ (Fig. 2d). To test the quantitative and predictable power of the Δq -GFA correlation, we fabricated the bulk $\text{Ir}_{10}\text{Ni}_{55}\text{Ta}_{35}$ and $\text{Ir}_{10}\text{Ni}_{50}\text{Ta}_{40}$ alloys by using conventional copper-mould suction casting where the cooling rate is roughly six orders of magnitude lower than the cooling rate during sputtering deposition²⁶. We observed that the $\text{Ir}_{10}\text{Ni}_{55}\text{Ta}_{35}$ and $\text{Ir}_{10}\text{Ni}_{50}\text{Ta}_{40}$ alloys with largest Δq measured on samples that were cooled with rates of roughly 10^9 K s^{-1} can be cast into fully amorphous rods of diameters even larger than 4 mm, exceeding the GFA of previously known BMG former of roughly 3 mm. To provide another example, $\text{Zr}_{46}\text{Cu}_{46}\text{Al}_8$ with a critical casting diameter of 8 mm has been reported as the alloy with the highest GFA in the ZrCuAl system³². However, $\text{Zr}_{50.75}\text{Cu}_{40.75}\text{Al}_{8.5}$ (indicated by the black dot in Fig. 3a) has recently been identified to form fully glassy rods with a diameter of 10 mm (ref. ³³). $\text{Zr}_{50.75}\text{Cu}_{40.75}\text{Al}_{8.5}$ falls right in the region of the largest Δq .

The ability to identify new BMGs exemplifies the power of the Δq -GFA correlation. For a more ‘quantitative measure’ of its

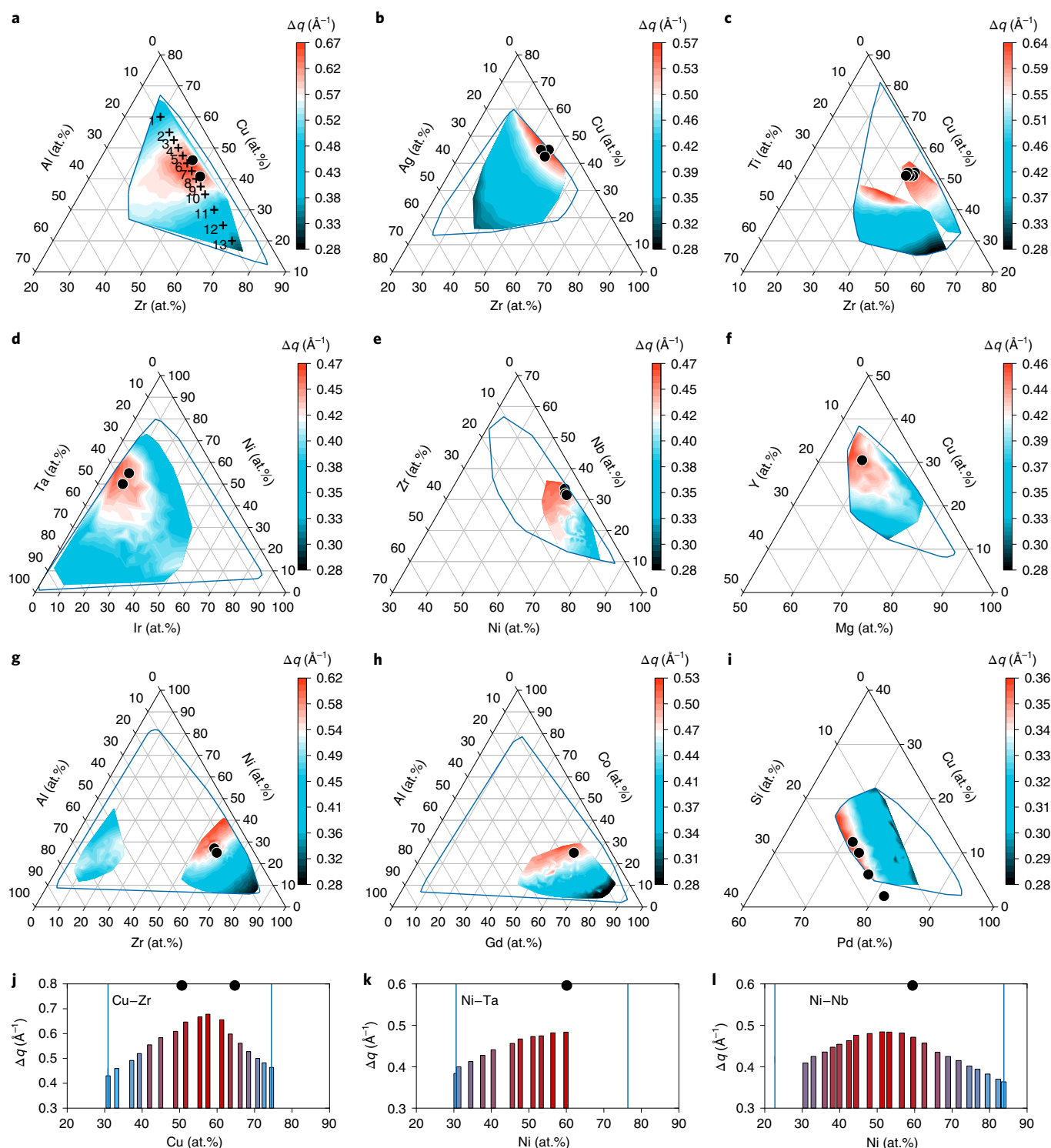


Fig. 2 | Correlation of Δq and GFA. Plot of Δq versus alloy composition for each here-considered alloy systems. **a–i**, ZrCuAl (**a**), ZrCuAg (**b**), ZrCuTi (**c**), IrNiTa (**d**), NiNbZr (**e**), MgCuY (**f**), ZrNiAl (**g**), GdCoAl (**h**) and PdCuSi (**i**) ternary alloy systems. **j–l**, Cu–Zr (**j**), Ni–Ta (**k**) and Ni–Nb (**l**) binary alloy systems. The black dots in the plots mark the alloys of the highest GFA in the corresponding alloy system^{13,20–24} that coincide with the composition of largest Δq . The solid blue lines envelope the compositions that have been covered in the combinatorial libraries. Alloys that are not fully amorphous have been excluded in this plot. The crosses indicated in **a** are the alloys for which molecular dynamics simulations were conducted as detailed in the Supplementary Materials.

effectiveness, we compare various alloy development strategies (Fig. 3). Specifically, we consider how many alloys have to be considered, fabricated and characterized to identify the best glass formers in an alloy system using conventional alloy development strategies, previously used combinatorial strategies and the here-proposed

integrated Δq –GFA correlation approach. We assume that a composition grid of 1 at.% is required for an alloy development strategy³⁴, and that roughly 5% of the roughly 5,000 alloys in a ternary system must be considered. This results in roughly 250 alloys for the identification of the best glass forming alloy within the alloy system.

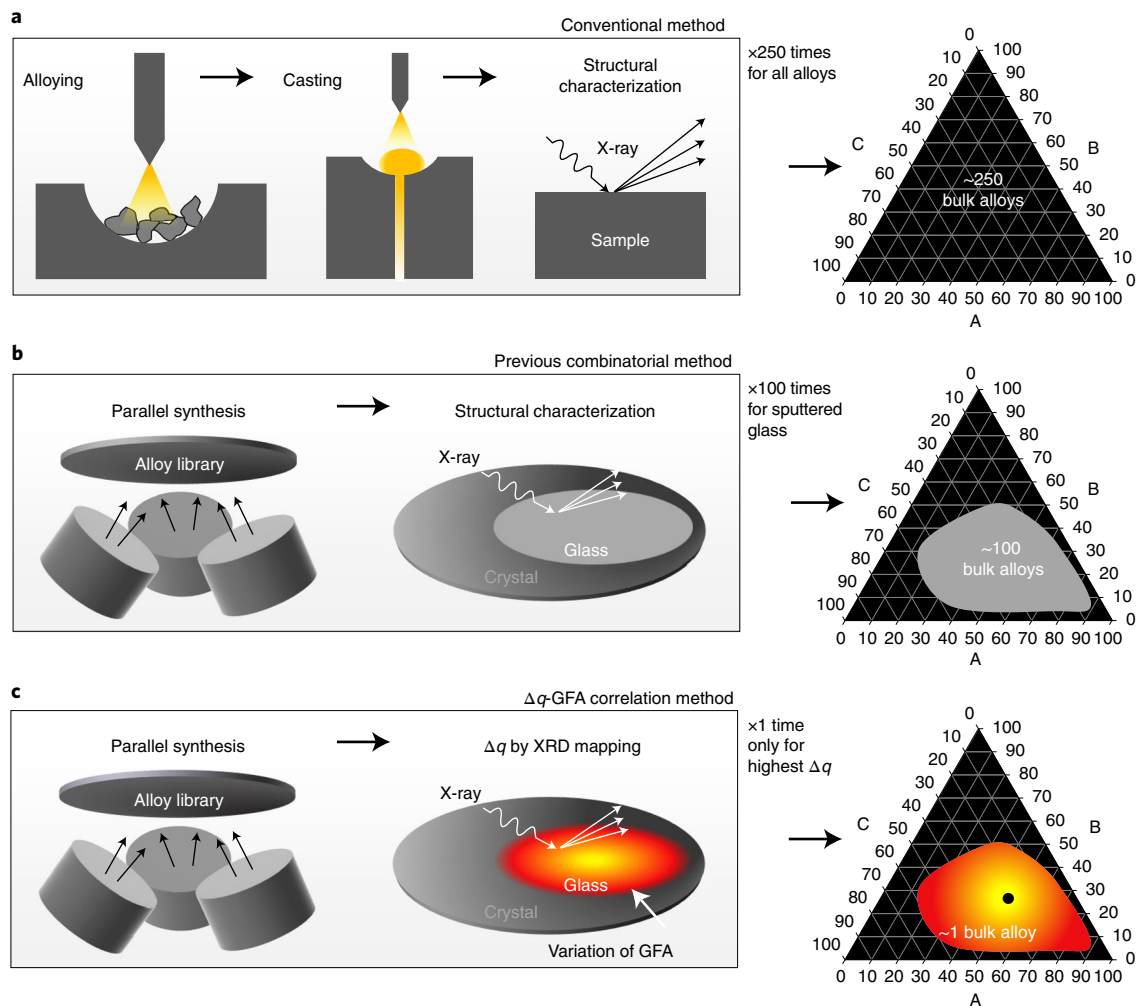


Fig. 3 | Effectiveness of the present and previous methods for BMG development. **a**, To identify best glass former in an alloy system, roughly 250 alloys have to be considered for GFA. The conventional approach includes alloying of each alloy individually, followed by subsequent controlled cooling and characterization. **b**, The number of alloys that have to be considered for bulk alloys can be reduced to roughly 100 with the combinatorial method, as the parallel synthesis and structural characterization can provide the binary information of glass versus crystal regions. **c**, With the present method based on Δq and GFA, the contour of Δq reveals glass formation tendency across the alloy system and substantially reduces the number of alloys. Bulk fabrication is only required for the alloy of largest Δq . To determine the absolute GFA, one only needs to consider roughly one bulk alloy for alloying, casting and characterizing.

Hence, with the conventional alloy development strategies, roughly 250 alloys have to be alloyed, cast and characterized (Fig. 3a). When using combinatorial approaches, all the alloys in one system can be fabricated simultaneously, and characterization can be carried out faster through scanning XRD methods that reveal binary information, that is, glass or crystal (Fig. 3b). The effectiveness of the methods scales with the ratio of the number of revealed glassy alloys to the number of alloys in the library. For alloy systems in consideration, a large portion, roughly 50%, of the alloys in the library form glasses during sputtering^{17,18,25}. The effectiveness of previous combinatorial strategies to identify BMGs is thus only about twice as high as the conventional method, as it still requires fabrication of roughly 100 bulk alloys through the conventional method.

For the here-proposed integrated Δq -GFA correlation approach, the XRD screening allows us to construct the contour of Δq , which unveils relative GFA within an alloy system (Fig. 3c). To determine the absolute value of the GFA, bulk fabrication is only required for the alloy of largest Δq . Therefore, compared to the roughly 100 bulk alloys with previous combinatorial strategies and around 250 bulk alloys with conventional strategies, the integrated Δq -GFA

correlation approach substantially reduces the number of alloys, for example roughly one bulk alloy, to be alloyed, cast and characterized. Hence, the integrated Δq -GFA correlation approach for the identification of the best BMG in an alloy system is around 250 times more effective than the conventional method, and around 100 times more effective than previous combinatorial strategies.

To ultimately test the predictability of the integrated Δq -GFA correlation approach, we select ZrCuCr as an alloy system that has not been considered for BMG formation. We sputter the ZrCuCr alloy library and perform XRD mapping; both tasks can be completed rapidly (Fig. 4a). We identify the alloy with the largest Δq within ZrCuCr system as $Zr_{43}Cu_{50}Cr_7$. This alloy is then fabricated through copper-mould suction casting and, as comparison alloys, $Zr_{40}Cu_{50}Cr_{10}$ and $Zr_{30}Cu_{55}Cr_{15}$ are fabricated as well. As shown in Fig. 4b, glassy rods with a diameter of 1.5 mm can be obtained with $Zr_{43}Cu_{50}Cr_7$, while the rods of $Zr_{40}Cu_{50}Cr_{10}$ and $Zr_{30}Cu_{55}Cr_{15}$ are completely crystalline. This indicates that $Zr_{43}Cu_{50}Cr_7$ has a higher GFA than the other two alloys. In addition to $Zr_{43}Cu_{50}Cr_7$, we identify $Ir_{20}Co_{40}Ta_{40}$ as a BMG-forming alloy in the unexplored IrCoTa system (Supplementary Fig. 10). The results of both ZrCuCr and

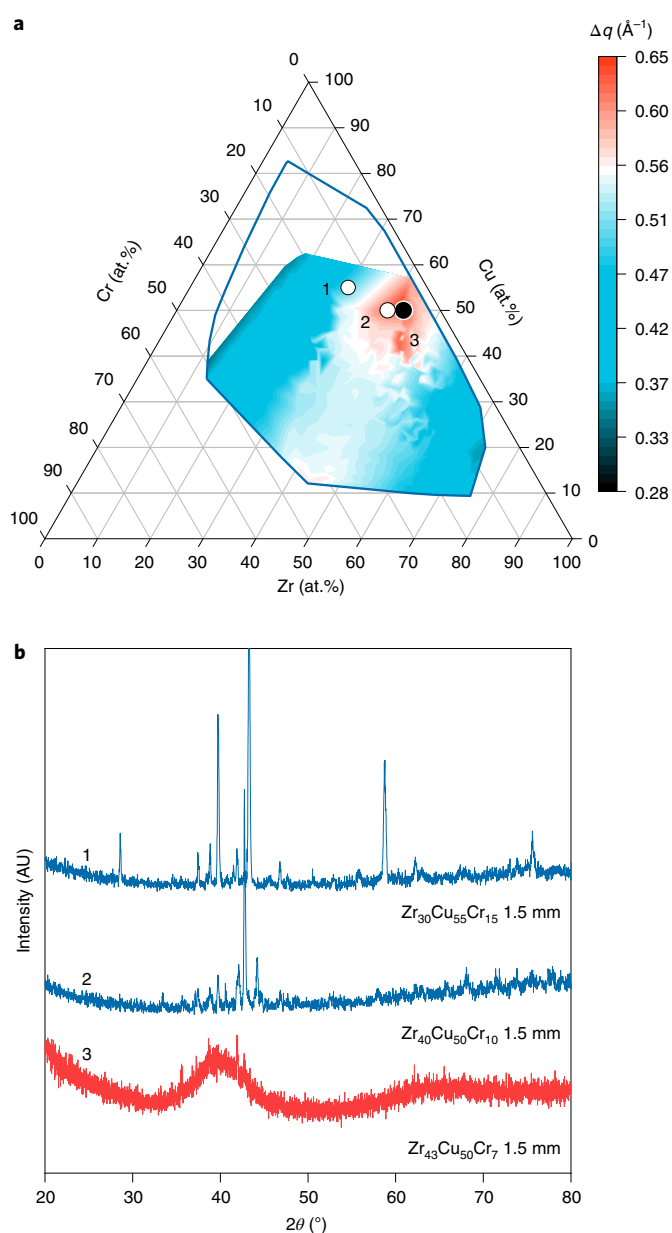


Fig. 4 | Example of Δq -GFA strategy to rapidly identify best glass former in an alloy system. **a**, XRD data on the ZrCuCr as-sputtered library revealed the region with the highest Δq . Alloy $\text{Zr}_{43}\text{Cu}_{50}\text{Cr}_7$ with the highest Δq and, as a comparison, $\text{Zr}_{40}\text{Cu}_{50}\text{Cr}_{10}$ with a medium Δq and $\text{Zr}_{30}\text{Cu}_{55}\text{Cr}_{15}$ with a small Δq were selected for bulk fabrication. **b**, XRD pattern on 1.5-mm rods fabricated through copper-mould casting reveals that $\text{Zr}_{43}\text{Cu}_{50}\text{Cr}_7$ has the highest GFA and is a BMG former, whereas the comparison alloys are both entirely crystalline, indicating a lower GFA.

IrCoTa further confirm the predictability of the Δq -GFA correlation for the identification of new BMGs.

Since the XRD pattern and Δq reflect the statistically averaged structural information of a glassy alloy, the continuous variation of Δq with compositions within an alloy system suggests that the compositional dependence of GFA in the system is related to the global atomic structure in the amorphous phase. For crystalline structures, the location of the diffraction peaks indicates the distances between periodic arrangements of structural units and the peak width is indicative of correlation length between the structural units. In an amorphous atomic arrangement, the broad hump peaks

in a diffraction pattern are defined by average atomic distances. As a statistic measure of the distance over which ordered arrangement of structural units can be maintained, the correlation length, which can be estimated with Δq through $L = 2\pi/\Delta q$, has been interpreted to reflect the degree of structural ordering of MGs^{35–37}. A larger Δq indicates a shorter correlation length, and thus an ordered arrangement of structural units can only be retained over small distance, indicating that the amorphous structure is statistically more disordered. To compare the correlation length across the considered alloy systems, L is normalized by the weighted average of atomic diameters, which yields the number of atoms across the correlation length (Fig. 5). When comparing the normalized correlation length for the here-considered alloy systems, a strong correlation reveals: alloys with high GFA and large Δq exhibit short correlation length within each of the system (solid circles in Fig. 5). The variation of correlation length indicates that in a system, alloys with high GFA possess highly disordered structures in their amorphous phases at least under rapid cooling, which are more disordered than other alloys in the system. It should be noted that the here-mentioned disordered structures refer to the statistic average of the global amorphous structure.

As the diffraction pattern only contains average information, we turn to simulations to understand the structural origin leading to the large Δq and structural disordering for alloys of high GFA. Since numerous simulations have been performed with ZrCuAl as a model alloy system^{11,38,39}, we modelled 13 ZrCuAl glass forming alloys with constant Al content, as marked by crosses in Fig. 2a (see Supplementary Information for details of the MD simulation). Δq of the ZrCuAl alloys vary non-monotonically with compositions (Fig. 6a). With the increase of Zr, the average coordination number of the first shell remains unchanged for the modelled alloys (Supplementary Fig. 11b). Numerous investigations have been carried out to understand GFA by focusing on local clusters of specific configurations, such as icosahedrons^{9,11,12,40,41}, which are present in most liquids^{42,43} and particularly pronounced in BMGs^{11,12,40,41} with a large negative heat of mixing among key constituents⁸. Our bond angle analysis on the modelled alloys indicates that the fraction of icosahedron- and crystal-like clusters either monotonically vary or remain essentially constant with the increase in Zr content (Supplementary Fig. 11c), suggesting that neither of them alone contributes to the high GFA reflected by a larger Δq in an alloy system. This is because the number of atoms organized in specific local clusters represents only a small fraction of the total^{38,39,44}. Instead, the atoms that are not involved in such clusters exhibit correlation with Δq , as their non-monotonic variation coincides with the variation of Δq for the modelled alloys (Fig. 6a and Supplementary Fig. 11c).

GFA is believed to relate with the small density difference between a glass and its crystalline counterpart²². A densely packed atomic structure is expected for strong glass forming alloys due to the prevalence of a few special local clusters. A disordered global structure characterized by a large Δq seems contrary to the expectation. To gain insight into the apparent contradiction, we further analysed the Voronoi polyhedron comprising the modelled glasses. Our analyses indicate that the fraction of the five most popular types of Voronoi polyhedra (Supplementary Table 1) vary inversely with GFA of the modelled alloys (Supplementary Fig. 11d). Except icosahedron and crystal-like clusters, our analyses reveal that far more types of polyhedra exist in the modelled glasses. The number of polyhedral types vary in a similar way to that for Δq (Fig. 6b), indicating that the alloy with a large Δq and high GFA comprise more types of cluster. MD simulations for MgCuY alloys also support the argument (Supplementary Fig. 12). From poor to good glass formers, the variation in the number of clusters is as large as roughly 20–30% for the modelled ZrCuAl (Fig. 6b) and MgCuY (Supplementary Fig. 12) alloys. This pronounced variation

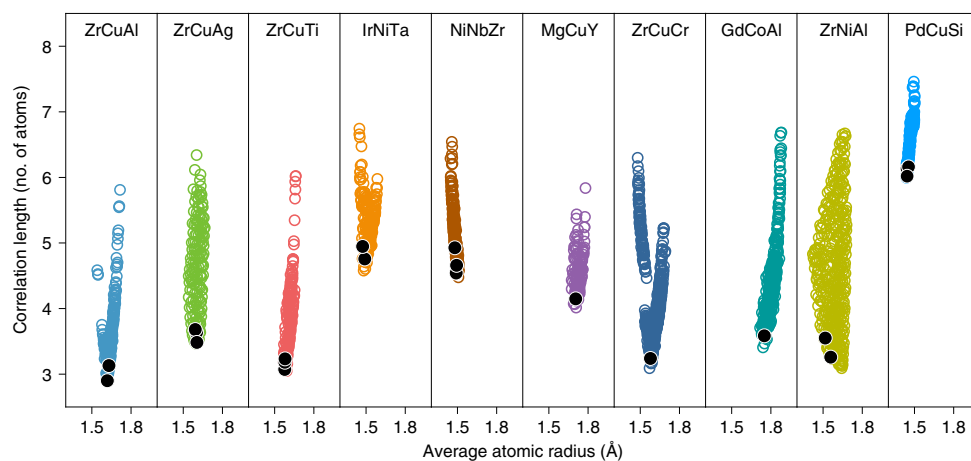


Fig. 5 | Correlation length evaluated by the number of atoms for the alloys identified as glass. The solid circles indicate the best glass formers in the corresponding alloy systems. The alloys of strongest GFA exhibit smaller correlation length quantified by the number of atoms across the length.

does reflect the large cluster dispersion in different alloys within an alloy system. Quasi-equivalence analysis can reduce the number of cluster types, but such analysis depends on cut-off values for classification. Here, we take the number of clusters identified with Voronoi tessellation as a measure of cluster dispersion. It would be insightful for future research to go beyond the here-used measure, and identify and quantify structural difference of the clusters, so that the subtle variation around the alloys of highest GFA can be further studied (Fig. 6b). Although local orders, in particular icosahedral clusters, have been considered to maximize the density of atomic packing, they are experimentally confirmed to be geometrically distorted⁴⁵. The distorted clusters lead to various unfilled space with diverse geometrical shapes that broadly distribute in the global amorphous structure^{10,46,47}. To achieve dense packing, incorporation of more types of polyhedra is necessary^{48,49}. As shown in Fig. 6c, maximal packing efficiency does emerge in the glasses that are composed of more types of cluster and exhibit large Δq . This indicates that it is not the packing density of individual clusters that determine the global packing efficiency, and that an enhancement of glass formation within one alloy system is achieved through an increasing distribution in local clusters. Because the atomic distances within each cluster differ from one type to another, the result is apparent global disordering due to the dispersity of structural units comprising the entire amorphous structure (Supplementary Fig. 13). Different from the disordering of a specific cluster, the dispersity induced global disordering results in efficient packing of the glass phase (Fig. 6c). Therefore, the varying GFA reflected by Δq in an alloy system, and the associated efficient space filling and dense atomic packing, can be explained by the difference in the number of involved polyhedral types, that is, dispersity of structural units comprising the amorphous structure. Our finding reveals that it is not the characteristics of specific short-range order, but the difference of short-range units that reflects GFA. The difference among the clusters includes but goes beyond cluster sizes.

Medium-range order has been widely used as a powerful concept to understand glass formation^{10,46,47}. However, numerous explanations have been assigned to the characteristics of medium-range order and the origin of the first diffraction peak^{10,46,47}. The ability to drastically simplify the structure–property relationship in crystalline solids originates from its periodicity and the ability to reduce the problem to small unit cells. Our large number of consistent experimental data indicate that GFA and the dispersion of local clusters are correlated. The strategy to reduce the problem to small ‘unit cells’, such as specific short-range orders, does not appear to

reflect the situation of liquids and glasses where lower energy states can be better realized through a wide dispersion of ‘units’. One could argue that this suggests a shift from the focus away from local clusters to understand glass formation to more holistic packing motifs. Our argument that the GFA of an alloy is governed by diverse structural units rather than a few types of cluster is consistent with the finding that existence of multiple clusters of dissimilar structures prevent each other from reaching the critical size for crystallization and thus facilitate the ease of glass formation⁵⁰.

It is surprising that the Δq –GFA correlation has not been revealed earlier, considering the fact that a large number of metallic glasses has been developed over the past 60 years. One main reason is that when characterizing Δq for the same alloy but with different alloy fabrication methods and/or XRD characterization methods, distinctly different values have been reported (Supplementary Fig. 14). Unlike previous work, our data-driven research is based on consistent parallel synthesis and characterization. Although the variation tendency of Δq is different from one alloy system to another (Fig. 1c), we argue that one could potentially compare Δq values for different alloy systems when the appropriate normalization factors have been identified. We speculate that data science approaches can play an important role in determining the normalization factors, which would ultimately allow computer-based alloy development.

In summary, through a data-driven approach considering roughly 5,700 alloys, we identified a correlation between GFA and the width of the first diffraction peak, Δq , in the XRD pattern. Such a correlation, observed here far away from equilibrium, suggests that within an alloy system the structural units are more dispersed in strong glass formers. The dispersity leads to apparent disordering but efficient packing of the amorphous structure. The discovery may shift our focus to understand glass formation from specific short-range orders to more holistic packing motifs and allows disruptive growths in the discovery of BMGs.

Online content

Any methods, additional references, Nature Research reporting summaries, source data, extended data, supplementary information, acknowledgements, peer review information; details of author contributions and competing interests; and statements of data and code availability are available at <https://doi.org/10.1038/s41563-021-01129-6>.

Received: 12 November 2020; Accepted: 13 September 2021;
Published online: 04 November 2021

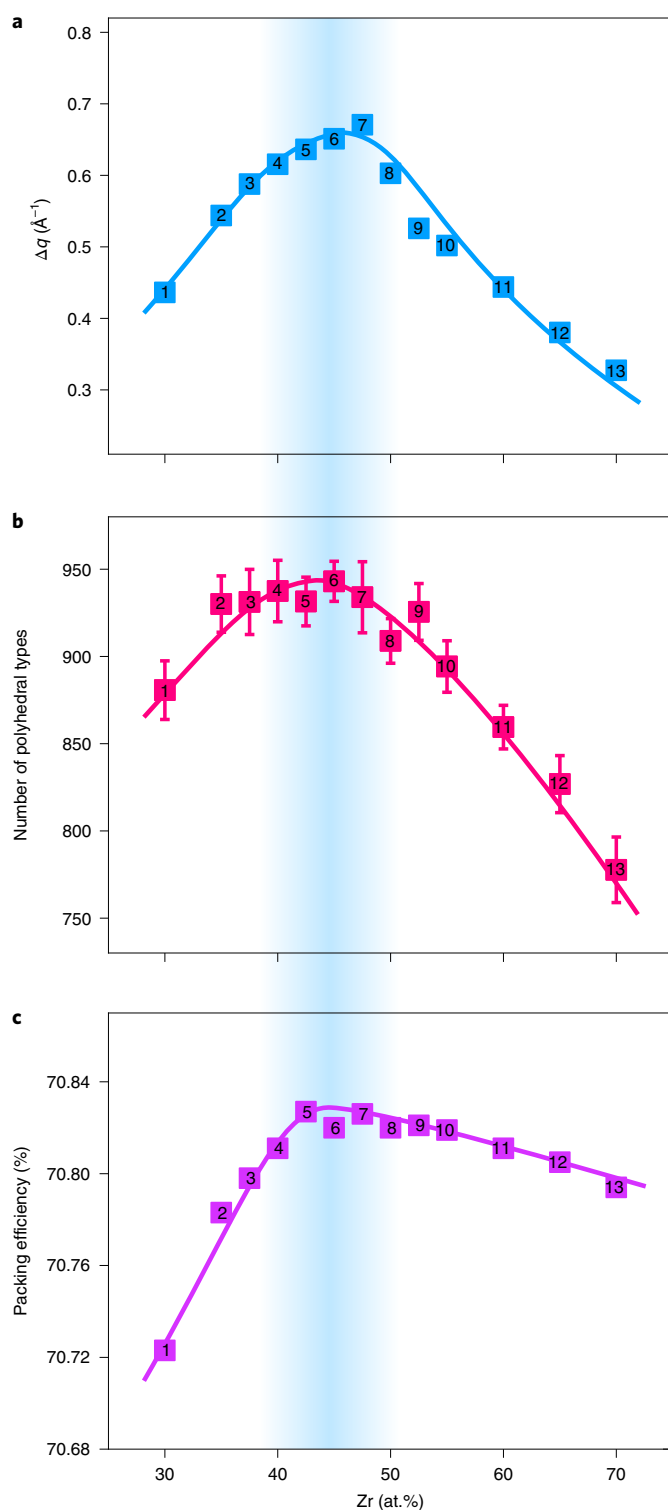


Fig. 6 | Comparison of experimentally measured Δq with structural characteristics revealed by molecular dynamics simulations for ZrCuAl alloys.

The amorphous structures are modelled and analysed for 13 ZrCuAl alloys with constant Al content but varying ratio between Zr and Cu. The system size for MD simulations is 40,000 atoms. **a**, Compositional dependence of experimentally measured Δq . **b**, Variation of the number of Voronoi polyhedral types with Zr content for the 40,000-atom MD models. **c**, Compositional dependence of packing efficiency for the 40,000-atom MD models. All the structural characteristics exhibit maximal values around $Zr_{45}Cu_{45}Al_{10}$, which have the highest GFA among the modelled alloys. In the plots, the number labels correspond to the labels in Fig. 2a, and the solid lines are guide for the eye.

References

- Greer, A. L. Metallic glasses. *Science* **267**, 1947–1953 (1995).
- Angell, C. A. Formation of glasses from liquids and biopolymers. *Science* **267**, 1924–1935 (1995).
- Debenedetti, P. G. & Stillinger, F. H. Supercooled liquids and the glass transition. *Nature* **410**, 259–267 (2001).
- Turnbull, D. Under what conditions can a glass be formed. *Contemp. Phys.* **10**, 473–488 (1969).
- Lu, Z. P. & Liu, C. T. Glass formation criterion for various glass-forming systems. *Phys. Rev. Lett.* **91**, 115505 (2003).
- Johnson, W. L. Bulk glass-forming metallic alloys: science and technology. *MRS Bull.* **24**, 42–56 (1999).
- Guo, S., Lu, Z. P. & Liu, C. T. Identify the best glass forming ability criterion. *Intermetallics* **18**, 883–888 (2010).
- Inoue, A. Stabilization of metallic supercooled liquid and bulk amorphous alloys. *Acta Mater.* **48**, 279–306 (2000).
- Jakse, N. & Pasturel, A. Glass forming ability and short-range order in a binary bulk metallic glass by ab initio molecular dynamics. *Appl. Phys. Lett.* **93**, 113104 (2008).
- Ma, D., Stoica, A. D. & Wang, X. L. Power-law scaling and fractal nature of medium-range order in metallic glasses. *Nat. Mater.* **8**, 30–34 (2009).
- Cheng, Y. Q., Ma, E. & Sheng, H. W. Atomic level structure in multicomponent bulk metallic glass. *Phys. Rev. Lett.* **102**, 245501 (2009).
- Fujita, T. et al. Atomic-scale heterogeneity of a multicomponent bulk metallic glass with excellent glass forming ability. *Phys. Rev. Lett.* **103**, 075502 (2009).
- Ashby, M. F. & Greer, A. L. Metallic glasses as structural materials. *Scr. Mater.* **54**, 321–326 (2006).
- Schroers, J. Processing of bulk metallic glass. *Adv. Mater.* **22**, 1566–1597 (2010).
- Saotome, Y., Itoh, K., Zhang, T. & Inoue, A. Superplastic nanoforming of Pd-based amorphous alloy. *Scr. Mater.* **44**, 1541–1545 (2001).
- Li, Y. L., Zhao, S. F., Liu, Y. H., Gong, P. & Schroers, J. How many bulk metallic glasses are there? *ACS Comb. Sci.* **19**, 687–693 (2017).
- Li, M. X. et al. High-temperature bulk metallic glasses developed by combinatorial methods. *Nature* **569**, 99–103 (2019).
- Ding, S. Y. et al. Combinatorial development of bulk metallic glasses. *Nat. Mater.* **13**, 494–500 (2014).
- Liu, J. B. et al. Fast screening of corrosion trends in metallic glasses. *ACS Comb. Sci.* **21**, 666–674 (2019).
- Zhang, H. T. et al. Combinatorial temperature resistance sensors for the analysis of phase transformations demonstrated for metallic glasses. *Acta Mater.* **156**, 486–495 (2018).
- McCluskey, P. J. & Vlassak, J. J. Glass transition and crystallization of amorphous Ni-Ti-Zr thin films by combinatorial nano-calorimetry. *Scr. Mater.* **64**, 264–267 (2011).
- Li, Y., Guo, Q., Kalb, J. A. & Thompson, C. V. Matching glass-forming ability with the density of the amorphous phase. *Science* **322**, 1816–1819 (2008).
- Deng, Y. P. et al. A combinatorial thin film sputtering approach for synthesizing and characterizing ternary ZrCuAl metallic glasses. *Intermetallics* **15**, 1208–1216 (2007).
- Schnabel, V. et al. Revealing the relationships between chemistry, topology and stiffness of ultrastrong Co-based metallic glass thin films: a combinatorial approach. *Acta Mater.* **107**, 213–219 (2016).
- Ren, F. et al. Accelerated discovery of metallic glasses through iteration of machine learning and high-throughput experiments. *Sci. Adv.* **4**, 1566 (2018).
- Liu, Y. H., Fujita, T., Aji, D. P. B., Matsuura, M. & Chen, M. W. Structural origins of Johari-Goldstein relaxation in a metallic glass. *Nat. Commun.* **5**, 3238 (2014).
- Yokoyama, Y., Yamasaki, T., Liaw, P. K. & Inoue, A. Study of the structural relaxation-induced embrittlement of hypoeutectic Zr-Cu-Al ternary bulk glassy alloys. *Acta Mater.* **56**, 6097–6108 (2008).
- Zhang, W. & Inoue, A. High glass-forming ability and good mechanical properties of new bulk glassy alloys in Cu-Zr-Ag ternary system. *J. Mater. Res.* **21**, 234–241 (2006).
- Dai, C. L., Guo, H., Li, Y. & Xu, J. A new composition zone of bulk metallic glass formation in the Cu-Zr-Ti ternary system and its correlation with the eutectic reaction. *J. Non-Cryst. Solids* **354**, 3659–3665 (2008).
- Zhu, Z. W., Zhang, H. F., Ding, B. Z. & Hu, Z. Q. Synthesis and properties of bulk metallic glasses in the ternary Ni-Nb-Zr alloy system. *Mater. Sci. Eng. A* **492**, 221–229 (2008).
- Ma, H., Zheng, Q., Xu, J., Li, Y. & Ma, E. Doubling the critical size for bulk metallic glass formation in the Mg-Cu-Y ternary system. *J. Mater. Res.* **20**, 2252–2255 (2005).
- Zhang, Q., Zhang, W., Xie, G. Q. & Inoue, A. Glass-forming ability and mechanical properties of the ternary Cu-Zr-Al and quaternary Cu-Zr-Al-Ag bulk metallic glasses. *Mater. Trans.* **48**, 1626–1630 (2007).
- Cui, X. et al. Centimeter-sized CuZrAl bulk metallic glass with good plasticity and chemical heterogeneity. *Intermetallics* **121**, 106773 (2020).

34. Na, J. H. et al. Compositional landscape for glass formation in metal alloys. *Proc. Natl Acad. Sci. USA* **111**, 9031–9036 (2014).
35. Elliott, S. R. Extended-range order, interstitial voids and the first sharp diffraction peak of network glasses. *J. Non-Cryst. Solids* **182**, 40–48 (1995).
36. Sinha, A. K. & Duwez, P. Radial distribution function of amorphous Ni-Pt-P alloys. *J. Phys. Chem. Solids* **32**, 267–277 (1971).
37. Sokolov, A. P., Kisluk, A., Soltwisch, M. & Quitmann, D. Medium-range order in glasses—comparison of Raman and diffraction measurements. *Phys. Rev. Lett.* **69**, 1540–1543 (1992).
38. Li, M., Wang, C. Z., Hao, S. G., Kramer, M. J. & Ho, K. M. Structural heterogeneity and medium-range order in ZrxCu100-x metallic glasses. *Phys. Rev. B* **80**, 184201 (2009).
39. Ward, L., Miracle, D., Windl, W., Senkov, O. N. & Flores, K. Structural evolution and kinetics in Cu-Zr metallic liquids from molecular dynamics simulations. *Phys. Rev. B* **88**, 134205 (2013).
40. Egami, T. & Waseda, Y. Atomic size effect on the formability of metallic glasses. *J. Non-Cryst. Solids* **64**, 113–134 (1984).
41. Ma, D. et al. Efficient local atomic packing in metallic glasses and its correlation with glass-forming ability. *Phys. Rev. B* **80**, 014202 (2009).
42. Frank, F. C. Supercooling of liquids. *Proc. R. Soc. Lon Ser.-A* **215**, 43–46 (1952).
43. Bernal, J. D. Geometrical approach to the structure of liquids. *Nature* **183**, 141–147 (1959).
44. Mattern, N. et al. Structural behavior of Cu_xZr_{100-x} metallic glass ($x=35-70$). *J. Non-Cryst. Solids* **354**, 1054–1060 (2008).
45. Hirata, A. et al. Geometric frustration of icosahedron in metallic glasses. *Science* **341**, 376–379 (2013).
46. Sheng, H. W., Luo, W. K., Alamgir, F. M., Bai, J. M. & Ma, E. Atomic packing and short-to-medium-range order in metallic glasses. *Nature* **439**, 419–425 (2006).
47. Miracle, D. B. A structural model for metallic glasses. *Nat. Mater.* **3**, 697–702 (2004).
48. Damasceno, P. F., Engel, M. & Glotzer, S. C. Predictive self-assembly of polyhedra into complex structures. *Science* **337**, 453–457 (2012).
49. Ma, E. Tuning order in disorder. *Nat. Mater.* **14**, 547–552 (2015).
50. Perim, E. et al. Spectral descriptors for bulk metallic glasses based on the thermodynamics of competing crystalline phases. *Nat. Commun.* **7**, 12315 (2016).

Publisher's note Springer Nature remains neutral with regard to jurisdictional claims in published maps and institutional affiliations.

© The Author(s), under exclusive licence to Springer Nature Limited 2021

Methods

Sample fabrication. The combinatorial thin film libraries were fabricated by confocal magnetron cosputtering (Ace Precision Machine, Inc., AFS1800) from elemental sputtering targets with purity better than 99.95%. Some 100-mm-diameter single-side-polished Si wafers were used as substrates. The composition gradient was controlled by tuning the sputtering power as well as the tilt angle of the sputtering guns. The thickness of the deposited films is about 1 μm . Bulk samples were prepared by arc-melting pure metals in Ar atmosphere, followed by copper-mould suction casting.

Materials characterizations. Compositions of the combinatorial libraries were measured by EDX attached to a Phenom scanning electron microscope. The measured compositions over the combinatorial libraries were calibrated by measurement on bulk alloys of known compositions by using EDX. The structure of the libraries was characterized by using a Malvern PANalytical Empyrean X-ray diffractometer with a Cu K α radiation source. To ensure fast screening, a PIXcel^{HD} linear detector containing 256 pixels in the detector array was used. A custom-designed sample stage attached to an xyz triaxial motor was used to realize XRD mapping, which was performed on a 19 \times 19 matrix covering the entire libraries with a spacing of 5 mm between each spot. At an incident angle of 15° where the first diffraction peaks are located, the X-ray spot size is 8 \times 6 mm² within which compositional variation of roughly 1–4 at.% for different elements. During XRD mapping, the movement of the sample stage is in the *xy* plane, which ensures the constant sample-to-detector distance for each location. The acquisition time for single XRD measurement is roughly 7 min. Across each library, 249 evenly spaced locations were characterized and more than one library was synthesized to cover different composition ranges for each investigated alloy system. The signal-to-noise level remains constant for the obtained XRD patterns (Supplementary Fig. 15). A kSA MOS UltraScan scanning curvature and stress measurement system was used to measure the local curvature of the substrate. The residual stress was calculated from the change in local curvature of the substrate before and after deposition, and the physical parameter of the substrate. The obtained values of residual stress were plotted with respect to the *x, y* coordinates on the wafer to generate the map of residual stress (σ) for the library.

Data availability

The authors declare that the data supporting the findings of this study are included within the paper and its Supplementary Information file.

Acknowledgements

We thank R. Zhao for experimental assistance in making the ZrCuCr master alloys. The work was financially supported by National Key Research and Development Program of China (grant no. 2018YFA0703600), National Natural Science Foundation of China (grant nos. 51825104, 51801230, 51801095, 11790291 and 61888102), CAS project (grant no. XDB30000000) and the Center for Materials Genome. J.S. and S.S. thank the NSF-DMR (grant no. 2104316).

Author contributions

Y.H.L. conceived and supervised the research. Y.H.L. and M.X.L. designed the research with advice from W.H.W. and J.S. M.X.L. and C.W. conducted the experiments with assistance from L.W.H. Y.T.S. and M.X.L. performed XRD pattern processing. Y.T.S. carried out molecular dynamics simulations. S.S. assisted in the literature review and preparation of bulk samples. All authors contributed to the analyses and interpretation of the data. M.X.L., Y.T.S., J.S. and Y.H.L. wrote the paper with input and comments from all authors.

Competing interests

The authors declare no competing interests.

Additional information

Supplementary information The online version contains supplementary material available at <https://doi.org/10.1038/s41563-021-01129-6>.

Correspondence and requests for materials should be addressed to Yan-Hui Liu.

Peer review information *Nature Materials* thanks S. Poon and the other, anonymous, reviewer(s) for their contribution to the peer review of this work.

Reprints and permissions information is available at www.nature.com/reprints.